Nucleation of MCM-41 Nanoparticles by Internal Reorganization of Disordered and Nematic-Like Silica – Surfactant Clusters**

Sajanikumari Sadasivan, Christabel E. Fowler, Deepa Khushalani, and Stephen Mann*

The synthesis of periodic mesostructures by self-assembly and cooperative organization of inorganic and organic species in aqueous media represents a significant benchmark in modern materials chemistry.[1–5] These template-directed processes generally involve charge matching interactions between inorganic oligomers and surfactant micelles,[6–8] and have been developed to produce a large number of hybrid mesophases and mesoporous replicas with surface areas of the order of 1000 $m^2 g^{-1}$. In spite of the advances in synthesis and applications of mesoporous materials, the mechanisms that give rise to periodic ordering in self-assembled hybrid systems are not well understood. Previous studies have focused on micellar structure just prior to precipitation,[9–12] or the growth of relatively large mesostructured crystals.[13–16] Details on the nucleation of the periodic mesophase have been difficult to obtain because of the relatively short timescales involved and the transient nature of the intermediates. Herein, we employ a controlled quenching process to sufficiently increase the nucleation period, such that high-resolution transmission electron microscopy (HR-TEM) can be used to reveal, for the first time to our knowledge, the structural stages associated with the nucleation of a hexagonally ordered silica – surfactant mesophase (MCM-41).

Recently, we reported the template-directed synthesis of single-domain MCM-41 nanoparticles with dimensions usually less than 150 nm by the controlled quenching of alkaline reaction mixtures containing tetraethoxysilane (TEOS) and cetyltrimethylammonium bromide (CTAB).[17] By employing a constant (40 s) dilution step, followed by variable time delays prior to arresting the reaction by instantaneous neutralization to pH 7 (see Experimental Section), we now show that it is possible to determine the structural and shape transformations of the nanoparticles during the onset and development of mesophase ordering. The earliest stage in this process was investigated by preparing samples using neutralization periods of less than 3 min. Small-angle X-ray diffraction (SAXRD) analysis showed an absence of long-range order with a broad low-angle reflection centered at 5.32 nm, consistent with swollen micelles and a low degree of silica condensation, and thermogravimetric analysis (TGA) measurements indicated that the hybrid mesophase contained 25 wt % of surfactant. Corresponding TEM images showed the presence of a homogeneous population of spherical nanoparticles with a mean size of 18 nm ($\sigma = 4$ nm). In contrast, extending the neutralization delay to 4 min produced a mixture of two types of nanoparticles, 75 % of which were spherical with increased mean diameter (35 nm, $\sigma =$ 9 nm), whereas the remaining 25 % were ellipsoidal and 67 ($\sigma = 16$) and 50 ($\sigma = 6$) nm in mean length and width, respectively.

Individual spherical nanoparticles up to about 50 nm in size were shown by high-resolution TEM imaging to consist of a loosely packed aggregate of disordered silica – surfactant micelles (Figure 1). The micelles were in the form of short rods, about 9.0 and 5.0 nm in length and width, respectively, that were "stained" by a 1 to 2 nm-thick surface layer of silica/silicate (Figure 1, arrow). Large numbers of nonaggregated spherical or slightly oblate silica-coated micelles were also imaged on the support film of the TEM grid (data not shown). Although drying artefacts cannot be ruled out, this suggests that for neutralization periods of less than 4 min the reaction mixture contained a high concentration of these discrete hybrid structures. In contrast with the disordered spherical aggregates, the ellipsoidal nanoparticles showed various degrees of internal mesostructural order. Ellipsoids that were relatively small (ca. 40 nm in length) had partially ordered interiors, which consisted of short rod-shaped silica-coated micelles preferentially aligned side-on within the nanoparticle (Figure 2 a). Although some end-on fusion of the rods parallel to the minor axis of the ellipsoids was apparent, the surfactant cylinders were in general too short to traverse the entire

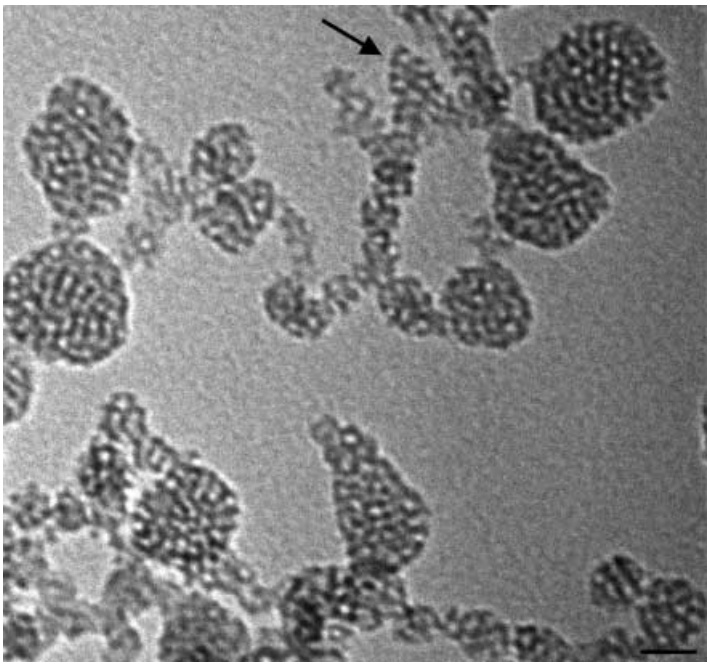

Figure 1. Initial stage in MCM-41 nucleation showing spherical clusters of disordered silica – surfactant micelles. Arrow highlights individual micelles. Scale bar = 20 nm.

[*] Prof. S. Mann, S. Sadasivan, Dr C. E. Fowler[+]
School of Chemistry
University of Bristol
Bristol BS8 1TS (UK)
Fax: (+44) 117-925-1295
E-mail: s.mann@bris.ac.uk
Dr D. Khushalani
School of Physical Sciences
University of Kent
Canterbury (UK)
[+] Current address: Forsyth Institute, 140 The Fenway, Boston MA 02115 (USA)

[**] We thank the University of Bristol for the support of an ORS award to S.S., and Dr. S. A. Davis for help with electron microscopy.

  1433-7851/02/4112-2151 $ 20.00+.50/0

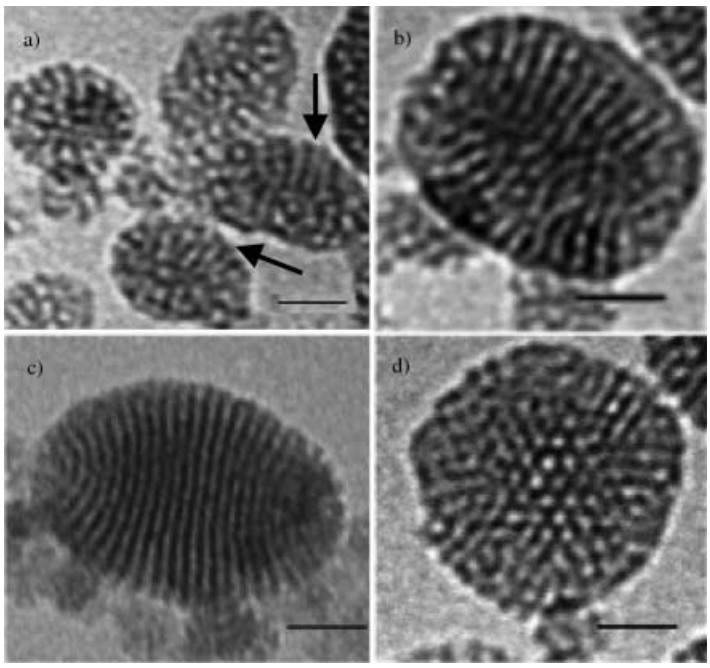

Figure 2. TEM lattice images of mesostructural ordering in oblate ellipsoidal nuclei. a) Side view of several nanoparticles, 40–50 nm in length, showing the initial stages of elongation and alignment of silica–surfactant cylinders around the periphery of the aggregated micelles (arrows). b) Side view of a 60-nm long nanoparticle showing increased levels of periodic order and central defects. c) Side view of a well-ordered single domain nanoparticle with modulated periodic mesostructure and local variations in the inter-micelle spacings. d) Top view along the radial axis showing hexagonal periodicity and 2D micelle cylinder alignment within the central regions of the nanoparticle ($d_{100} = 4.4$ nm, $a = 5.1$ nm). Scale bars = 20 nm in all micrographs.

nanoparticle. Instead, localized domains of micelle alignment and extension in length were observed predominantly in the near surface regions of the nanoparticles (Figure 2a, arrows). In contrast, larger ellipsoids that were around 60 nm in length showed a progressive increase in the internal ordering such that the silica-micelle cylinders were extended almost across the whole nanoparticle to produce a single-domain periodic mesostructure with localized defects (Figure 2b). Similar images were obtained for ellipsoids between 60 and 100 nm in length except that the lattice fringes were continuous throughout the ellipsoids (Figure 2c). Interestingly, as shown in Figure 2c, the nanoparticle interiors consisted of an unusual bilateral arrangement of parallel silica–surfactant cylinders that became progressively more curved in an outward direction with increasing displacement from the centre of the ellipsoid. As a consequence, the *d* spacings increased by about 30% from 4.2 nm in the central regions to 5.1 nm at the particle edges.

Field-emission gun scanning electron microscopy (FEGSEM) and TEM images recorded along different projections indicated that the ellipsoidal nanoparticles were flattened spheres (oblate ellipsoids) with a diameter/thickness aspect ratio of about 1.3:1. Thus, the oval-shaped images shown in Figure 2a–c correspond to side-on projections whereas a view along the radial axis (top view) was associated with nanoparticles that appeared circular in shape. The latter only showed well-ordered 2-D hexagonal dot patterns—corresponding to the [001] channel direction—in the central regions of the nanoparticles (Figure 2d), which is consistent with the structural modulation observed in the side views. Moreover, the hexagonal lattice patterns were only observed for ellipsoids greater than about 60 nm in width, suggesting that this is the approximate critical size for the onset of long-range MCM-41 periodicity.

Extending the neutralization period to 9 min produced no internally disordered spherical nanoparticles and increased the monodispersity, as well as the mean diameter and thickness (120 ($\sigma = 19$) and 80 ($\sigma = 18$) nm, respectively), of the oblate ellipsoids, which were present in almost 100% yield. The marginal increase in aspect ratio from 1.3:1 to 1.5:1 with growth suggests that the addition of silica–surfactant micelles from the supersaturated solution occurs preferentially by side-on fusion around the radial axis of the oblate ellipsoids. This flattens the ellipsoids further, which reduces the curvature of the surface and associated internal bending of the silica–surfactant cylinders, with the consequence that disklike nanoparticles with small hexagonal faces were observed by FEGSEM. Corresponding TEM studies showed no significant changes in the internal organization of the modulated silica–surfactant mesostructure, although the lattice images were more well-defined, suggesting an increase in the degree of silica condensation. This was consistent with XRD measurements, which showed a single broad reflection with a *d* spacing centered at 4.40 nm, and TGA measurements that indicated no change in the surfactant composition (25 wt%).

The above results suggest the following model for the nucleation of MCM-41 nanoparticles under the highly specialized conditions investigated (Figure 3). Initially, the reaction mixture is at pH 13 for 40 s, which initiates TEOS hydrolysis and the formation of soluble silicate species that interact with

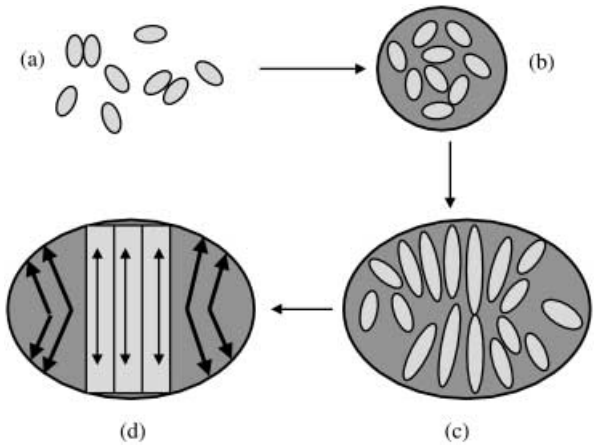

Figure 3. Schematic representation showing proposed mechanism for the nucleation of MCM-41 nanoparticles. a) Solution phase containing short rod-shaped silica-coated CTAB micelles. b) Aggregation of silica–surfactant micelles into disordered spherical nanoparticles less than 50 nm in size. c) Internal reorganization to nematic-like silica–surfactant mesostructure due to side-on ordering and cylinder elongation, and associated change in the particle morphology to an oblate ellipsoid. d) Elongation of the silica–surfactant micelles to produce single-domain nanoparticles with modulated mesostructure. Arrows indicate the local orientation of the micelle cylinders.

  1433-7851/02/4112-2152 $ 20.00+.50/0

the cationic headgroups of the CTAB micelles. Subsequent dilution reduces the pH spontaneously to around 12, which in turn decreases the rate of hydroxide-catalyzed hydrolysis, lowers the solubility of the silicate precursors, and reduces the surface charge on incipient silica–surfactant clusters present in the medium. In addition, the 85% decrease in concentration reduces the rate of cluster coalescence sufficiently that silica–surfactant micelles at various stages of aggregation can be investigated. Significantly, the individual micelles are not highly elongated as proposed in previous models of MCM-41 formation, but short rods with aspect ratios of about 1.7:1. This is consistent with recent studies using liquid-state NMR and fluorescence spectroscopy, which indicated that CTAB micelles were not significantly changed in the presence of silicate species at high pH.[18–20]

Aggregation of the individual silica-coated micelles produces spherical nanoparticles with disordered interiors and "raspberry-like" external morphology (Figure 3b). Nucleation of the periodic mesostructure occurs by internal reorganization of a disordered cluster of a few hundred loosely packed silica-coated micelles (particle diameter < 50 nm) and is associated with two stages involving the interactive coupling of structural and morphological transformations. In the first stage, side-on ordering and wall formation between the micelles produce a nematic-like silica–surfactant interior that initiates a sphere to oblate ellipsoid transformation such that the director field lies approximately parallel to the radial axis (Figure 3c). The intimate association between particle morphology and internal structure explains the preferential ordering in the near surface regions and alignment of the partially elongated micelle cylinders around the minor axis of the oblate ellipsoid. In the second stage, the shape anisotropy induced by side-on ordering of the silica–surfactant micelles becomes coupled with the subsequent structural development of the hexagonally ordered interior. As the surface to volume ratio is high, the energy required to bend the hexagonal array of silica–surfactant cylinders away from the principal director field is offset by the surface alignment of the channel directions normal to the local tangent (Figure 3d). Thus, as the cylinders increase in length and extend across the entire nanoparticle, the corresponding mesostructure becomes progressively modulated about the radial axis due to changes in the local curvature of the ellipsoids.

In conclusion, our results indicate that under our experimental conditions the nucleation of MCM-41 nanoparticles occurs heterogeneously by a disorder–order phase transition within silica–surfactant micellar aggregates less than 50 nm in size. A similar mechanism has been recently proposed for large particles of mesostructured silica although no direct structural observations were reported.[21] In our system, the onset of 2D periodicity occurs through a nematic-like intermediate that is associated with a structure-induced shape transformation. In turn, the oblate ellipsoidal morphology influences the subsequent extension and structural reorganization of the micelle cylinders to produce a modulated hexagonal silica–surfactant periodic mesophase. Further work using organo-functionalized nanoparticles is in progress to determine the generality of this nucleation mechanism.

Experimental Section

Typically, the nanoparticles were synthesized by using the following molar ratios: 0.12 CTAB:0.5 NaOH:1 SiO_2:130 H_2O. CTAB (0.8 g) was dissolved in an alkaline solution consisting of 1M NaOH (10 g) in H_2O (35.1 g) and TEOS (3.78 g) added under stirring. After 40 s (dilution delay) the reaction mixture was added to water (300 g) and left stirring for various time periods (1 to 10 min, neutralization delay) before 2M HCl was added to neutralize the solution. Stirring was stopped when the pH had decreased to 7.0, after which samples were taken directly from the reaction mixture and air-dried onto grids for TEM or field-emission gun scanning electron microscopy (FEGSEM) analysis. The dilution step reduced the reaction pH from 13 to 12.2, and subsequent neutralization delays of 1, 3, 4, 6, and 10 min corresponded to further decreases in the pH to 12.0, 10.6, 10.3, 10.25 and 10.3, respectively. The concentration of CTAB after dilution (6×10^{-3}M) remained above the critical micelle concentration.

Solid samples were obtained by evaporation of the water from the reaction mixture in air for 24 h and analyzed by small angle X-ray diffraction (SAXRD) and thermogravimetric analysis (TGA). The surfactant template was removed by calcination at 540 °C.

Received: December 18, 2001 [Z18408]

[1] C. T. Kresge, M. E. Leonowicz, W. J. Roth, J. C. Vartuli, J. S. Beck, *Nature* **1992**, *359*, 710–712.
[2] J. Y. Ying, C. P. Mehnert, M. S. Wong, *Angew. Chem. Int. Ed.* **1999**, *111*, 58–82; *Angew. Chem. Int. Ed.* **1999**, *38*, 56–77.
[3] F. Schüth, *Chem. Mater.* **2001**, *13*, 3184–3195.
[4] C. Sanchez, G. J. D. A. Soler-Illia, F. Ribot, T. Lalot, C. R. Mayer, V. Cabuil, *Chem. Mater.* **2001**, *13*, 3061–3083.
[5] A. Stein, B. J. Melde, R. C. Schroden, *Adv. Mater.* **2000**, *12*, 1403–1419.
[6] A. Firouzi, D. Kumar, L. M. Bull, T. Besier, P. Sieger, Q. Huo, S. A. Walker, J. A. Zasadzinski, C. Glinka, J. Nicol, D. Margolese, G. D. Stucky, B. F. Chmelka, *Science* **1995**, *267*, 1138.
[7] Q. S. Huo, D. I. Margolese, G. D. Stucky, *Chem. Mater.* **1996**, *8*, 1147–1160.
[8] S. H. Tolbert, C. C. Landry, G. D. Stucky, B. F. Chmelka, P. Norby, J. C. Hanson, A. Monnier, *Chem. Mater.* **2001**, *13*, 2247–2256.
[9] M. F. Ottaviani, A. Galarneau, D. Desplantier-Giscard, F. Di Renzo, F. Fajula, *Microporous Mesoporous Mater.* **2001**, *23*, 1–8.
[10] H. P. Lin, C. P. Kao, C. Y. Mou, *Microporous Mesoporous Mater.* **2001**, *23*, 135–141.
[11] F. Di Renzo, D. Desplantier, A. Galarneau, F. Fajula, *Catal. Today* **2001**, *66*, 73–77.
[12] H. Naono, M. Hakuman, T. Tsunehisa, N. Tamura, D. Nakai *J. Colloid Interface Sci.* **2000**, *224*, 358–365.
[13] S. Che, Y. Sakamoto, O. Terasaki, T. Tatsumi, *Chem. Mater.* **2001**, *13*, 2237–2239.
[14] F. Kleitz, F. Marlow, G. D. Stucky, F. Schuth, *Chem. Mater.* **2001**, *13*, 3587–3595.
[15] H. Yang, G. A. Ozin, C. T. Kresge, *Adv. Mater.* **1998**, *10*, 883–887.
[16] W. Zhou, J. Klinowski, *Chem. Phys. Lett.* **1998**, *292*, 207–212.
[17] C. E. Fowler, D. Khushalani, B. Lebeau, S. Mann, *Adv. Mater.* **2001**, *13*, 649–652.
[18] L. Sicard, J. Frasch, M. Soulard, B. Lebeau, J. Patarin, T. Davey, R. Zana, F. Kolenda, *Microporous Mesoporous Mater.* **2001**, *23*, 25–31.
[19] J. Frasch, B. Lebeau, M. Soulard, J. Patarin, R. Zana, *Langmuir* **2000**, *16*, 9049–9057.
[20] R. Zana, J. Frasch, M. Soulard, B. Lebeau, J. Patarin, *Langmuir* **1999**, *15*, 2603–2606.
[21] H. B. S. Chan, P. M. Budd, T. deV. Naylor, *J. Mater. Chem.* **2001**, *11*, 951–957.

  1433-7851/02/4112-2153 $ 20.00+.50/0